Progress in Organic Coatings 167 (2022) 106861

Contents lists available at ScienceDirect

Progress in Organic Coatings

journal homepage: www.elsevier.com/locate/porgcoat

Bio-based one-component epoxy resin: Novel high-performance anticorrosive coating from agro-industrial byproduct

Lucas R.R. da Silva [a], Bruna A. Carvalho [b], Rita C.S. Pereira [b], Otilio B.F. Diogenes [a], Ursula C. Pereira [a], Kássia T. da Silva [a], Walney S. Araujo [a], Selma E. Mazzetto [b], Diego Lomonaco [b,*]

[a] Department of Metallurgical and Materials Engineering, Federal University of Ceara, 60440-900 Fortaleza, CE, Brazil
[b] Department of Organic and Inorganic Chemistry, Federal University of Ceara, 60440-900 Fortaleza, CE, Brazil

ARTICLE INFO

Keywords:
Organic coating
EIS
Corrosion protection
Bio-based coatings

ABSTRACT

In this present work, an epoxy resin produced from an agroindustrial byproduct, cashew nutshell liquid (CNSL), was used for manufacturing a one-component anticorrosive epoxy coating. CNSL-based epoxy resin (e-CNSL) was synthesized using a solvent-free methodology with performic acid generated *in situ*. The chemical structure of resin was evaluated by FTIR and ^{1}H NMR. The curing parameters of the epoxy-phenol system with 1-methylimidazole (1-MIM) as an accelerator were investigated by differential scanning calorimetry (DSC). The use of only 5% by weight of 1-MIM was efficient to catalyze the reaction, obtaining the lowest cure temperature (150 °C). The coating showed high crosslinking and good thermal-mechanical performance, where the initial decomposition temperature was 200 °C and glass transition temperature was 30 °C. The anti-corrosive performance of e-CNSL/MIM5 exposed to salt spray and 3.5% w/v NaCl solution was monitored by electrochemical impedance spectroscopy, adhesion, and visual evaluation during the exposure period. Humidity test with visual evaluation was also performed. The coating presented high impedance module at 10^{8} Ω.cm^{2} and high adhesive property, suffering low delamination during the tests. Thus, the one-component bio-based coating developed is promising to be applied for corrosion protection purposes.

1. Introduction

Organic coatings are one of the most efficient protection technologies against corrosion processes, a major problem in several fields around the world, representing a serious security concern with huge financial losses.

This has been the most widely used preventive measure today, especially in transport and infrastructure sector, with a market cost forecast for 2022 of US$31 billion [1]. These materials have excellent properties that enable their use in a wide variety of industries. They are flexible, impact resistant, have chemical resistance and they act as a physical barrier directly protecting metallic substrates from aggressive environments, requiring simple and economical application, with easy repair and maintenance [2].

Epoxy resins represent the largest part of the coatings market, because of its versatility. These resins have an excellent combination of mechanical properties, adhesive capacity, dimensional stability, thermal and chemical resistance [3]. In addition, epoxy resins can be used in other segments, such as adhesives, composites, building materials, laminates and insulators [4]. The global market epoxy resins size reached US$25.8 billion in 2018 and is projected at about US$34 billion until 2022 [5].

However, approximately 90% of commercially available epoxy resins are synthesized from petrochemical resources, using bisphenol A (BPA) as a precursor to bisphenol A diglycidyl ether epoxy resin (DGEBA). BPA is produced by condensing acetone with phenol. Its annual global production was estimated at around 10 million tons in 2020 [5,6].

Studies have shown that BPA presents severe risks to human health. Due to its phenolic structure, BPA is similar to estrogen, being able to bind to receptors for this hormone, and impair some bodily functions, such as growth, embryonic development and cell regeneration, and trigger endocrine disorders [7,8]. Thus, there is an urgent need to develop new materials from renewable and non-toxic resources that

* Corresponding author.
E-mail address: lomonaco@ufc.br (D. Lomonaco).

https://doi.org/10.1016/j.porgcoat.2022.106861
Received 18 October 2021; Received in revised form 30 March 2022; Accepted 4 April 2022
Available online 10 April 2022

reduce dependence on fossil fuels, and provide significant contributions to environmental sustainability.

The literature reports the use of renewable sources as epoxidized precursors in the development of partially/fully bio-based thermoset polymers with good thermomechanical properties. Ammar and collaborators [9] used epoxidized soybean oil in the development of a fully organic-multifunctional coating system with good film transparency and good properties of hardness, adhesion, thermal stability and physical barrier against corrosion. Parvathy et al. [10] synthesized bioresins from silanized castor oil (SCO) and silanized methyl ricinoleate (SMR) for the development of a green, sustainable, hydrophobic biocoating for paper substrate and with recyclability potential.

Among the aromatic renewable sources, the literature reports the use of epoxidized lignin for total replacement of BPA in the formulation of epoxy resins, obtaining a thermoset polymer with thermal stability and thermomechanical performance comparable to that of the epoxy system based on DGEBA [11]. As an aromatic epoxidized oil, the literature reports the total epoxidation of the cardanol side-chain providing a way to eliminate the pendant ends of the chain that cause low *Tg* of cardanol-derived polymers [12]. Other authors made use of cashew nut shell liquid (CNSL) in the synthesis of epoxy resin for asphalt binders and antioxidants for biodiesel [13,14].

The CNSL is a low-cost and underutilized agro-industrial byproduct, but has a rich chemical composition composed mainly of phenols *meta*-substituted with a long unsaturated alkyl chain, which is responsible for its oily texture. The structural characteristics of CNSL enable its operation as a versatile platform for chemical modifications, representing a promising route in the development of tailor-made renewable polymers. It is worth mentioning that, since CNSL is an inedible oil, it does not present competition in the food supply chain and because it comes from raw material waste, it does not compete for production land, unlike other vegetable oils (edible) [15].

CNSL is characterized as a dark, viscous, and caustic oil, extracted from spongy shell that covers the cashew kernels of *Anacardium occidentale* L. Cashew tree is a tropical tree native to Brazil, grown mainly on the continents of Asia (India, Vietnam, and Indonesia), Africa and South America. The world production of cashew nuts in 2017/2018 crop reached around 789 thousand tons [16].

This agroindustrial byproduct corresponds to 25% of the nut weight and can present different chemical compositions according to the extraction method, and thus classified into two types: natural or technical. Natural CNSL is obtained by solvent extraction and is composed of anacardic acid (60–70%), cardol (10–20%), cardanol (3–10%), 2-methylcardol (2–5%), and other minor constituents. On the other hand, technical CNSL is obtained after industrial treatment, under high temperatures, during the processing of almonds, which results in a low added value waste, consisting mainly of cardanol (60–70%) and cardol (10–20%), 2-methylcardol (2–5%) and polymeric materials (5–10%) [17].

The use of cardanol, obtained from the distillation of technical CNSL, has shown satisfactory results as a promising renewable source in the manufacture of products for different applications, as in plasticizer for PLA and PVC [18,19], lubricating oils [20], phenalkamine curing agents [21], as well as the use of commercial cardanol (Cardolite) in the synthesis of novolac phenolic resins [22], epoxy resins [23], flame retardants [24] and polyurethanes for coating [25].

However, distilled cardanol still has approximately 6% of cardol and, depending on the application, it is necessary to carry out a second distillation to obtain a high purity material, increasing energy expenditure [26]. So, there is growing concern about the sustainability and energy efficiency of this chemical process, as raised by circular economy guidelines.

Although raw CNSL also has the potential to replace phenol, its use as an alternative raw material, without isolating its components or performing any purification treatments, has been little explored. Thus, this work aims to synthesize a technical CNSL-based epoxy resin, to produce an organic coating through a one-component system, using 1-methylimidazole as a catalyst, as well as studying thermal properties and its anticorrosive performance.

2. Materials and methods

2.1. Materials

Cashew nutshell liquid (CNSL) was supplied by Amêndoas do Brasil LTDA (Fortaleza-CE, Brazil). All reagents were used as received: sodium bicarbonate, hydrogen peroxide (35%), ethyl acetate, Amberlite IR-120H, and acetone were supplied by Synth. Formic acid (85%), xylene (99%), 1-methylimidazole (99%), crystal violet (for microscopy), and 33% wt. hydrobromic acid in acetic acid were supplied by Sigma.

2.2. Epoxidation of CNSL

The epoxidation of double bonds of CNSL was performed according to the methodology described by Silva et al. [27] with some modifications (Fig. 1).

CNSL (100.00 g), formic acid (18.02 g, 0.333 mol), and Amberlite IR-120H (20.00 g, 20 wt% of CNSL) were added to a 1 L beaker. The mixture was cooled to 0 °C in an ice bath and stirred at 80 rpm with a mechanical stirrer system for 5 min. Then, 35% v/v H_2O_2 (190.0 mL, 2.217 mol) was added dropwise over 1 h. At the end of the addition, the mixture was heated at 60 °C for 5 h and continuously stirred at 120 rpm. The molar unsaturation ratio of CNSL: formic acid: hydrogen peroxide was 1:0.5:3.33. The progress of the reaction was monitored by thin layer chromatography.

After the reaction was complete, the organic phase was separated from the aqueous phase and diluted with ethyl acetate (1 L). Then, Amberlite IR-120H was recovered by vacuum filtration and the product was neutralized with saturated sodium bicarbonate solution (3 × 30 mL) and washed with distilled water until neutral pH. The organic phase was collected and dried with anhydrous sodium sulfate and concentrated under reduced pressure, obtaining 90.0 g of a reddish-brown viscous liquid (yield of 90% in relation to the weight of CNSL, and 57.4% conversion of double bonds considering the initial iodine number, as describe Table 1).

2.3. Preparation of test specimens

The specimen was prepared with the addition of 1.5 g of e-CNSL resin, 1 mL of acetone and 5% wt of 1-methylimidazole (MIM5) in a beaker and stirred for 5 min. The solution was poured into a mold of silicone (4 cm × 2 cm × 2 cm) and subjected to vacuum degassing for 1 h. The sample was allowed to dry for 24 h and submitted to a controlled temperature program: 100 °C, 130 °C for 1 h each and 150 °C for 2 h. The cured samples were conditioned at room temperature for 24 h and then analyzed by gel content, FTIR, TGA and DSC.

2.4. Surface preparation

1010 steel panels (10 cm × 15 cm) had their surfaces treated with G-25 steel shot followed by cleaning with acetone before applying the coating. The panels had a roughness of 50 μm and were measured by PosiTector®SPG equipment.

2.5. Application and curing of coatings

The e-CNSL/MIM5 coating was prepared using xylene as diluent (30% w/w with respect to e-CNSL resin) and 1-methylimidazole as accelerator (5% w/w with respect to e-CNSL resin), thereby obtaining a viscosity of 6.62 Pa.s for application on steel panels with the aid of a 500 μm extender. The coated substrates were placed in an oven at 70 °C for 1 h for solvent evaporation, and then, they were submitted to the same

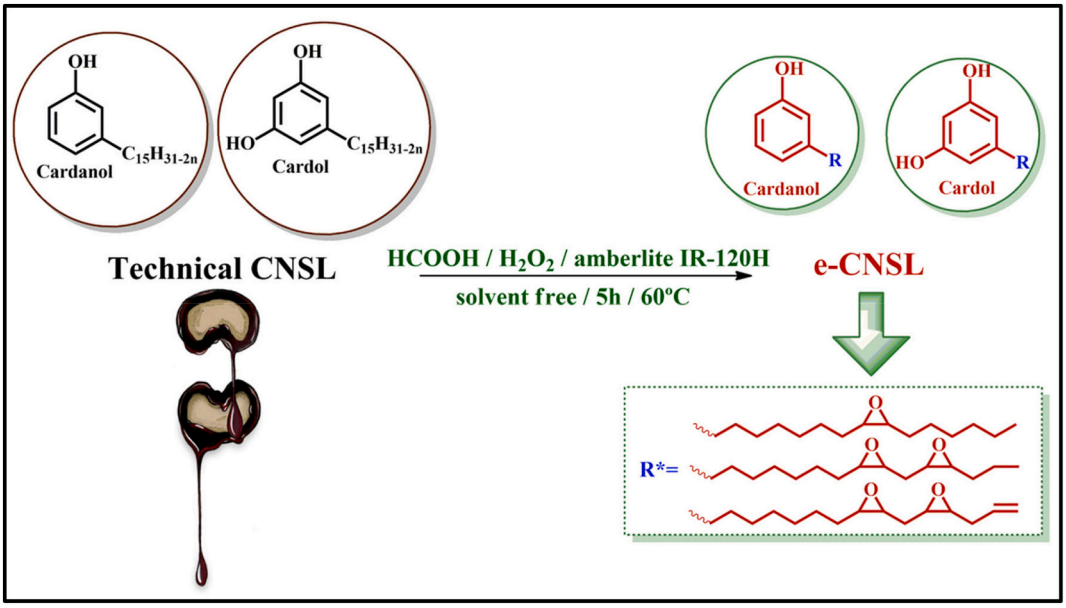

Fig. 1. Functionalization of CNSL by epoxidation reaction through the generation of performic acid *in situ*.

Table 1
Chemical and rheological characterization of CNSL and e-CNSL resins.

Samples	Iodine value (g/100 g)	Epoxy content (mmol/g)	EEW (g/eq)	Viscosity (Pa. s)
CNSL	169± 0.0	–	–	0,2
e-CNSL	72 ± 1	2.24 ± 0.1	446 ± 1	621

controlled temperature program, described in Section 2.3. The coated panels were conditioned at room temperature for 24 h to then be evaluated for their adhesive and anti-corrosion properties.

2.6. Characterization techniques and test methods

2.6.1. Characterization of CNSL and e-CNSL epoxy resin

The iodine values of CNSL and e-CNSL resin were determined by titration according to the procedure reported by Tubino and Aricetti [28]. The epoxy equivalent weight (EEW), weight percent of epoxide (E) and the epoxy content (EC) of the resin were determined by the titration method according to ASTM D1652 with adaptation [27]. The determination was carried out in triplicate for each sample. The EEW of the resin was calculated using Eq. (1):

$$EEW\left(\frac{g}{eq}\right) = \frac{(43\ or\ 42) \times 100}{E} \quad (1)$$

Where 43 refers to the molar weight of the glycidyl epoxy ring or 42 refers to the disubstituted epoxy group and weight percent of epoxide (E) calculated using Eq. (2):

$$E = \frac{(4.3\ or\ 4.2) \times V \times N}{w} \quad (2)$$

Epoxide Content (EC) was calculated according to Eq. (3):

$$EC\left(\frac{mmol}{g}\right) = \frac{(V \times N)}{w} \quad (3)$$

Where V is the volume of HBr used to titrate the sample in mL, N is the normality of HBr solution in mol L^{-1}, and w is the weight of the sample in g.

Fourier transform infrared spectroscopy (FTIR) was performed on a FRONTIER FT-IR/NIR Perkin Elmer in attenuated full reflectance (ATR) mode with zinc selenide crystal (ZnSe). The wavelength range of analyzes was 4000–550 cm^{-1} with a resolution of 4 cm^{-1} and 32 scans.

The chemical structure of e-CNSL resin was further confirmed by NMR analysis carried out in a Bruker Avance DPX 300 spectrometer operating at 300 MHz for ^1H nuclei, at room temperature, using deuterated chloroform ($CDCl_3$) as solvent. The e-CNSL (30 mg) was dissolved in 0.4 mL of $CDCl_3$-*d* and the residual solvent signal was used as the internal reference (7.27 for ^1H).

Viscosity measurements were carried out on an RST-CPS Brookfield Rheometer, using a 50 mm diameter cone-plate geometry with 0.045 mm gap, with shear stress from 100 to 2000 Pa at 25 °C.

2.6.2. Properties of the test specimens

Gel content (GC) was determined by gravimetric analysis based on ASTM D2765 with modifications. Samples of cured films (Wi) with a mass of 30 mg were immersed in chloroform (3 mL) for 24 h to extract the soluble content. After this period, the samples were dried at room temperature to constant weight (Wf). The analysis was performed in triplicate, and the GC of the samples were calculated using Eq. (4):

$$GC(\%) = \frac{Wf}{Wi} \times 100 \quad (4)$$

These values express in percent the non-soluble gel content that can be correlated with a crosslink density formed in polymers.

The thermal behavior was studied by thermogravimetric analysis (TGA, Mettler-Toledo TGA/SDTA851e). For TGA analysis, 5 mg of sample were heated from 30 °C to 800 °C in an atmosphere of N_2 and from 30 °C to 800 °C under an atmosphere of synthetic air (50 mL min^{-1}) at a rate of 10 °C min^{-1}.

For the polymerization study, the samples were evaluated by differential scanning calorimetry (DSC, Mettler-Toledo DSC 823e) by heating from 30 °C to 400 °C at a heating rate of 10 °C min^{-1}. For evaluation of glass transition temperature (*Tg*) of coating, 5 mg of sample were heated from 30 °C to 150 °C, cooled from 150 °C to −30 °C and heated from −30 °C to 150 °C under a heating rate 20 °C min^{-1}. Both methods were carried out under a nitrogen atmosphere (50 mL min^{-1}).

2.6.3. Coating properties

The thickness of the coatings was measured with PosiTector® 6000 equipment. The coatings were tested for pull-off adhesion properties

using the PosiTest AT-A Automatic Adhesion Tester (DeFelsko – Type V model) according to ASTM D4541-17 (Test Method E) [5]. For the adhesion test, an aluminum dolly was glued to the surface of coating cured with two-component epoxy glue with a drying period of 24 h. Then a cut of the coating was carried out around the dolly. The rupture stress was registered after the detachment between coating and substrate. The adhesion tests were performed three times to verify the repeatability of the measurements. The percentage of adhesive and cohesive failures resulting from the adhesion test was estimated using the free software ImageJ to calculate the areas related to each type of failure.

The water contact angle (WCA) of coating was determined using a WCA instrument (GBX Instrumentation Scientification) with measurements made in triplicate. The images were recorded with a camera (Nikon PixeLINK) attached to the WCA equipment for short periods. The optical properties (brightness values) were also evaluated by a T&M268 triangular brightness meter (GLOSS METER) with measurements at 20°, 60° and 85° angles. The measuring range in the 20°/60° angle is 0–1000 GU and in the 85° angle is 0–160 GU according to the equipment specifications. The equipment is always calibrated before taking measurements. Measurements after equipment calibration were performed on e-CNSL/MIM5 coated over 1010 steel plates. These measurements were performed before electrochemical tests and accelerated tests.

2.6.4. Anti-corrosion properties

The corrosion protection behavior of coating was studied using three different methods:

2.6.4.1. Immersion test. The corrosion resistance properties of e-CNSL/MIM5 coating were evaluated using electrochemical impedance spectroscopy (EIS) study on the AUTOLAB PGSTAT302P potentiostat. A conventional system of three electrodes was used, in which silver/silver chloride electrode, platinum electrode and coated panels were used as reference, counter and working electrodes, respectively. The surface area of the working electrode exposed to the test solution (3.5% w/v NaCl) was 21.22 cm^2 in all cases at a temperature of 22 °C for 35 days. A sinusoidal potential disturbance of 25 mV was applied in the 1×10^5 - 6×10^{-3} Hz frequency range.

2.6.4.2. Resistance to salt spray test and humidity. The corrosion resistance properties of coatings were evaluated by exposing the coated steel panels, with a single scratch on the bottom of the plate, to a 5% w/v sodium chloride (NaCl) aqueous solution at 35 ± 2 °C for 33 days according to ASTM B-117. The equipment used was a Q-FOG cyclic corrosion chamber from Q-Lab. Before testing, the edges and backs of the coated samples were covered with water-resistant tape. The tested panels were exposed to continuous spraying of salt solution placed at an angle of 30° in the chamber. The corrosion in the area marked were inspected for signs of bubbles, stains and loss of adhesion.

The effect of humidity on a completely cured coating was studied by placing the coated panels in a humidity chamber model BASS-UK-S-01/2012 (BASS Equipament Ltd) for 44 days, in accordance with ISO 6270-2. The humidity chamber was maintained at 95% relative humidity and a temperature of 40 ± 3 °C. After the test was completed, the exposed panels were evaluated for the appearance or not of visible damage.

3. Results and discussion

3.1. Characterization of e-CNSL

The successful synthesis of e-CNSL epoxy resin was confirmed by chemical, rheological and spectroscopic analyzes. The iodine values, epoxy content and viscosities of CNSL and e-CNSL are shown in Table 1. The iodine value of the e-CNSL resin reduces when compared to the CNSL, confirming that there was a conversion of the internal unsaturations present in the aliphatic chains of cardanol and cardol into oxirane groups by epoxidation reaction. The conversion was 57.4% according to Eq. (5):

$$\%Conversion = \frac{100 \times (IV0 - IVF)}{IV0} \quad (5)$$

Where IV0 is the initial iodine value of the CNSL and IVF is the iodine value of the e-CNSL resin.

Epoxy contents found in the literature of epoxy resins derived from CNSL, as well as DGEBA resins, are higher than those found in this work [23,29,30]. This difference is due to the difference in the resin synthesis mechanism. DGEBA epoxy resins and other CNSL derivatives reported in the literature are synthesized by glycidylation occurring in phenolic hydroxyls, whereas for e-CNSL epoxidation occurs only in double internal bonds since the double terminals of the molecule are not effectively epoxidized by the method formic acid/hydrogen peroxide [23], which decreases the number of oxirane groups per mass of resin.

Viscosity measurements were performed for CNSL and e-CNSL at 25 °C and shear stress of 2000 Pa, given in Table 1. The viscosity values show that the side chain epoxidation increased the viscosity in relation to CNSL, due to the addition of epoxy groups to the side chain, which reduces the mobility of the chain and increases the polarity, and possibly because of the oligomerization of the components of the e-CNSL during epoxidation [23].

3.2. Spectroscopic measurements

Through FTIR analysis, it was observed the changes that occurred during the synthesis of the epoxy resin, evaluating the disappearance and appearance of absorption bands characteristic related to the structure of CNSL and e-CNSL resin, as also observed in the literature [31].

In Fig. 2, in CNSL spectrum is possible to observe a broad band related to the phenolic hydroxyl group at 3354 cm^{-1}; stretches in 3009 cm^{-1} of C—H bonds for the unsaturated side chain present in the constituents of CNSL, as well as stretches of C—H for the methyl, methylene and methine groups at 2924, 2853 and 1456 cm^{-1}; in addition to the stretching in 1595 cm^{-1} of C = C bonds present in the aromatic ring.

In the e-CNSL resin spectrum was observed a symmetrical stretching of C—O (1200 cm^{-1}), appearance of an asymmetric stretching band of the epoxy ring (826 cm^{-1}) and complete disappearance of the band in 3009 cm^{-1} related to the C—H stretching of the side chain internal unsaturations after epoxidation, suggesting that double bonds were converted into oxirane groups. However, it is possible to observe a C═O band at 1724 cm^{-1} that possibly refers to the opening of the epoxy ring by formic acid [32].

Fig. 3 shows ^1H NMR spectra of CNSL and its epoxidized product e-CNSL, respectively. Its main structural modifications can be identified and used as evidence of effective formation of oxirane rings as already reported in previous work [27] and in literature [23,33].

The signals observed at 6.26 ppm and in the range of 6.7–7.2 ppm are attributed to the aromatic protons of cardol and cardanol, respectively. The epoxidation of the side chain is confirmed by displacement of the signals in the range of 5.3–5.5 ppm (internal unsaturation protons **j**) in the CNSL spectrum to 2.9 and 3.2 ppm (protons **n**), related to hydrogens of oxirane ring, in the e-CNSL spectrum. This indicates the conversion of internal double bonds of the side chain into epoxy groups during the epoxidation reaction. In addition, the altered chemical displacement of peaks in the range of 1.3–1.7 ppm (protons **f** and **g**) also supports the formation of epoxy groups.

However, there were no significant changes in the multiplets in the range of 5.0–5.2 ppm and 5.8–5.9 ppm, which correspond to the protons of the terminal double bonds of the side chain (protons **l** and **m**), that can still be observed in e-CNSL spectrum. This shows that the terminal double bonds are less reactive and the synthetic method used is not efficient, thus requiring other reaction conditions for epoxidation [12].

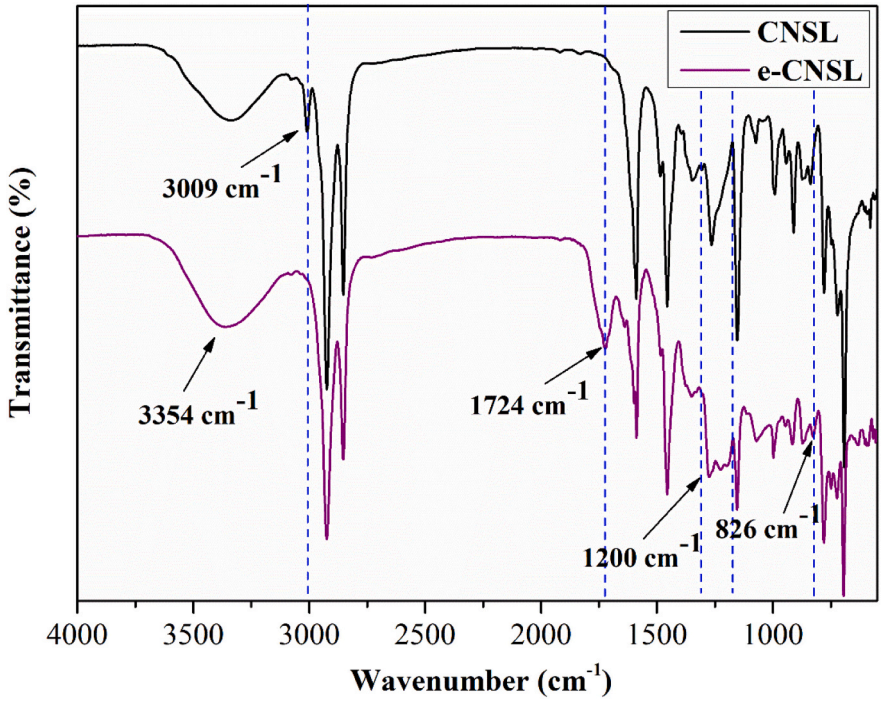

Fig. 2. FTIR spectra of CNSL and e-CNSL.

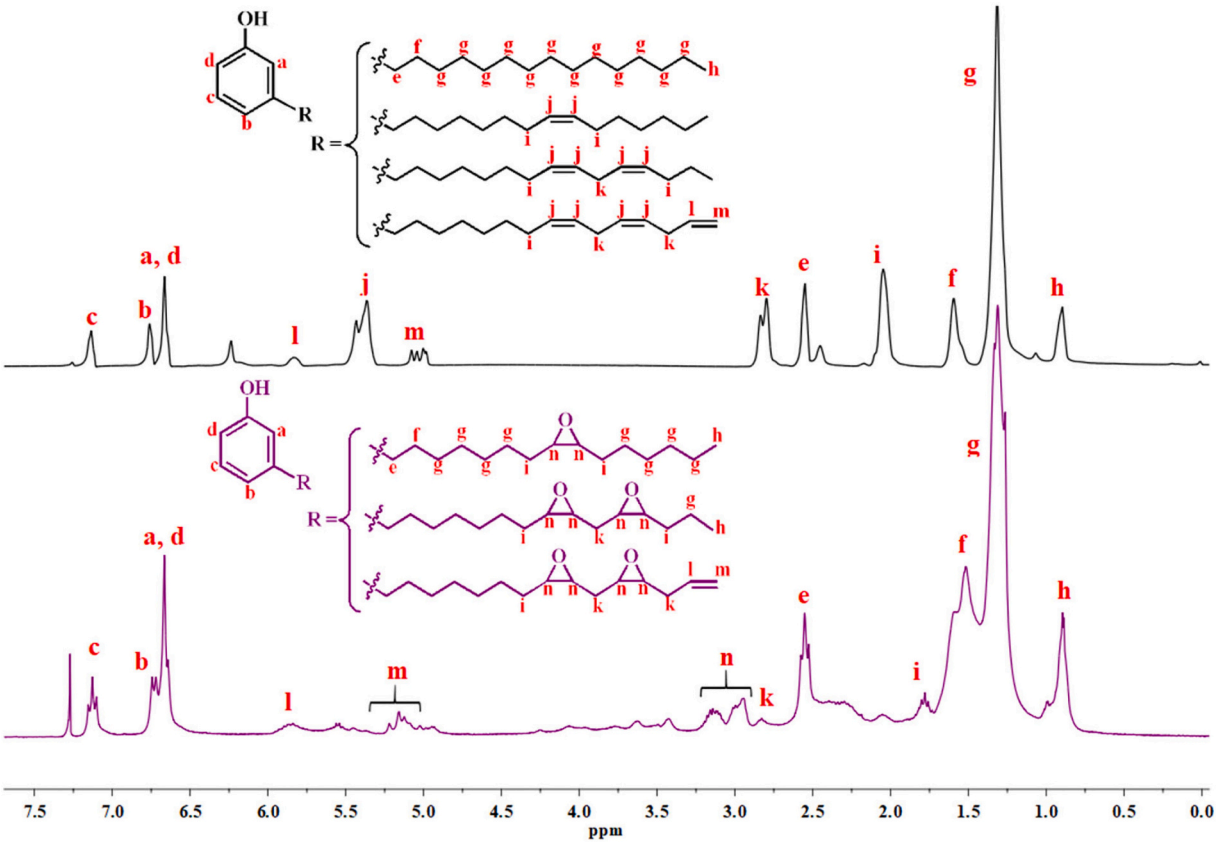

Fig. 3. ^{1}H NMR spectra of CNSL and e-CNSL.

This behavior, in which the band at 3009 cm^{-1} referring to the double bonds disappears while in the ^{1}H NMR spectrum the signals of the double terminals still remain, is also observed in the literature [12,34]. Signals between 3.3 and 3.75 ppm are secondary hydroxyl protons suggesting that there were epoxy ring opening reactions.

The conventional epoxidation method is complex, problematic and of low selectivity, involving several reactions simultaneously in the aqueous, organic phases and in the water-oil interphase [35,36]. Among

these reactions, epoxy ring opening can occur as a secondary process in the organic phase and in the interphase. This is due to the presence of water, formic acid and hydrogen peroxide, in addition to the phenolic molecules present in CNSL, which can act as ring-opening agents (Fig. 4) [37].

Thus, the characterization data obtained suggest that the epoxy resin may contain in its structure secondary hydroxyl groups, formate groups and oligomers, even in small amounts. This may explain why the epoxy content was lower than expected, as well as obtaining a resin with high viscosity.

3.3. Study of polymerization of e-CNSL resin with catalyst

Through the DSC analysis, preliminary polymerization studies were carried out to evaluate the effect of concentration of 1-MIM (0%, 1%, 2.5%, 5% and 10% w/w).

Fig. 5 shows the thermograms of mixtures (e-CNSL/1-MIM) with different amounts of 1-MIM and the data obtained from analysis, such as starting polymerization (T_{onset}), peak temperature polymerization (T_p) and polymerization enthalpy (ΔH_{pol}) are summarized in Table 2.

As can be seen in Fig. 5, two exothermic peaks were observed in all samples corresponding to the epoxy ring-opening reaction, as well as the polymerization of the terminal double bonds of cardanol and cardol side chain, possibly followed by a degradation process above 330 °C. Notably, the temperature of curing exothermic peak without catalyst was very high (286 °C), indicating that the reactivity of the curing reaction between the phenols present in the e-CNSL and the epoxide groups is extremely low.

According to the literature, phenolic curing agents such as phenol [38], bisphenol A [39], tannic acid [40], and quercetin [41] required temperatures above 200 °C for the ring-opening reaction. Therefore, to increase the reaction reactivity and consequently reduce the curing temperature of e-CNSL, the 1-MIM accelerator was added in different proportions.

The thermograms of the 1% to 10% samples are similar. When the concentration of 1-MIM increases from 1% to 10%, T_{onset} decreases about 28 °C from 120 °C to 92 °C because the reaction rate is associated with a higher concentration of catalyst. This is also observed for T_p, which decreased by 45 °C.

Conversely, when the concentration of the accelerator increased by up to 10%, ΔH_{pol} increased, possibly due to a greater extent of the etherification reaction by cardanol and cardol. It is quite clear that the difference between the temperatures of T_{onset} and T_p between the concentrations of 5% and 10% were not so significant, so it was decided to use only 5% of 1-MIM for production of coatings.

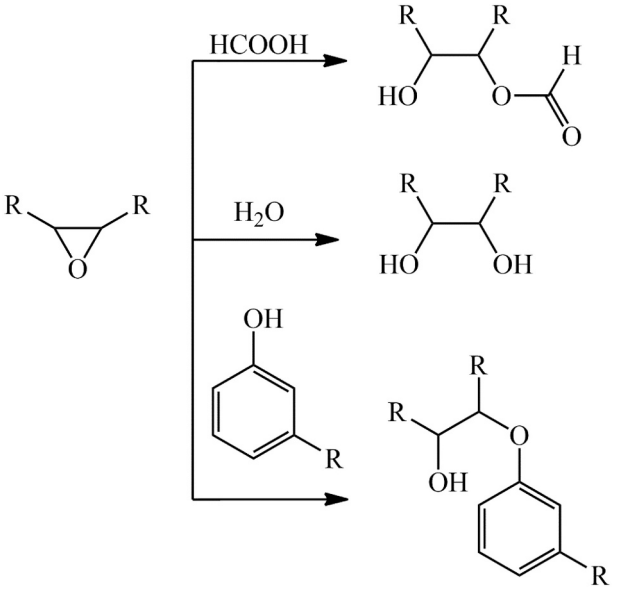

Fig. 4. Secondary reactions in the epoxidation process.

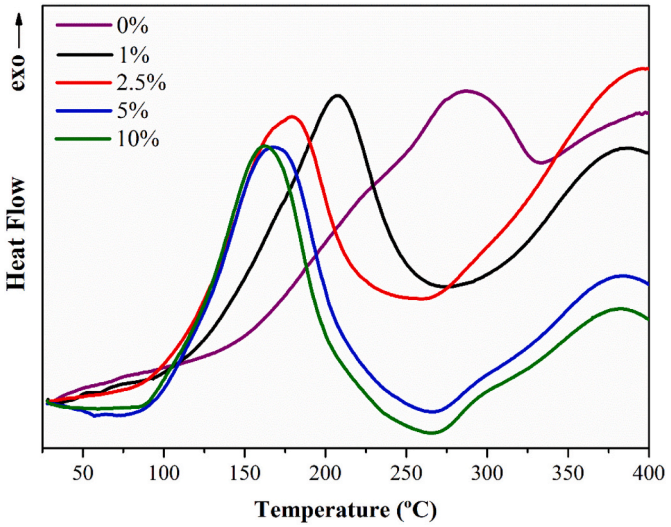

Fig. 5. DSC thermograms of e-CNSL with different concentrations of 1-MIM.

Table 2
T_{onset} and T_p temperatures of epoxy resins polymerization.

e-CNSL/1-MIM	0%	1%	2,5%	5%	10%
Onset (°C)	148	120	111	98	92
Peak T (°C)	286	207	179	167	162
Enthalpy (J/g)	−107	−153	−137	−185	−188

3.4. Characterization of specimens

3.4.1. Spectroscopic measurements

In Fig. 6 are shown the FTIR spectra in the fingerprint region of e-CNSL resin and its polymer completely cured at 150 °C to verify the conversion of functional groups. The aryl alkyl ether Ar-O-C stretch band was observed at 1255 cm^{-1} in the e-CNSL/MIM5 spectrum, as well as a C-O-C stretch at 1051 cm^{-1} [42]. In addition it is possible to observe

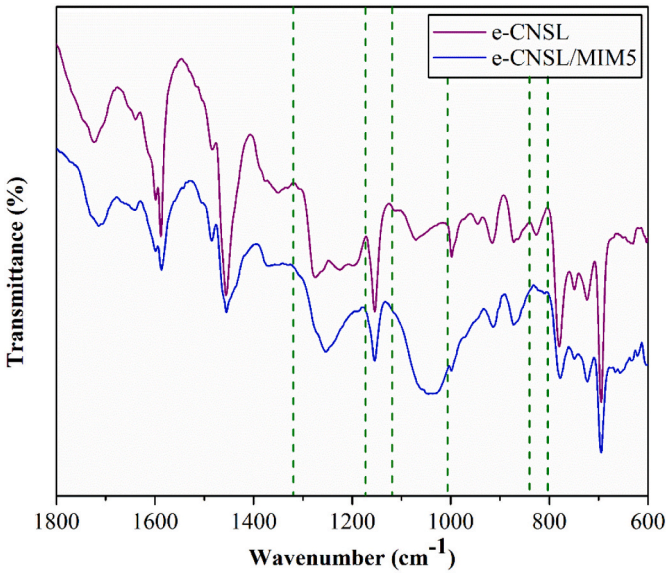

Fig. 6. FTIR spectra of the epoxy resin and the cured coating.

the disappearance of 826 cm^{-1} band referring to the epoxy group [43]. The set of data presented confirms the structural formation of the polymer proposed in this work.

3.4.2. Free film properties

The gel content was measured in order to study the extent of curing of the e-CNSL/MIM5 coating. The gel content found was 95.4 ± 0.3%, confirming the almost complete crosslinking of coating. This probably indicates that it still contains non-crosslinked chains, such as non-functionalized or saturated cardanol chains, or open epoxy groups during the epoxidation reaction as can be seen by FTIR of pure epoxy resin, which can increase the soluble parts and consequently present below 100%.

The thermal behavior of cured coating was analyzed by DSC and TGA techniques. The glass transition temperature (*Tg*) found for the polymer was 30 °C, which is very high when compared to our previous work using epoxy resin e-CNSL with other hardeners [27]. The use of imidazole as a catalyst provides materials with a polymeric network with high rigidity according to Yang and collaborators [4]. This behavior is the result of a higher crosslinking density previously seen by the GC forming a more compact network that reduces the segmental and chain mobility of final structure of copolymer.

The decomposition temperatures of the uncured resin and the coating were investigated by analyzing TGA under atmospheres of N_2 and Air. The resulting thermograms and their first derivative curves are shown in Fig. 7. The temperatures at 5% loss of mass, 30% loss of mass and the maximum rate of decomposition were calculated and denoted as $T_{d5\%}$, $T_{d30\%}$ and T_{dmax} (°C), are described in Table 3. The coating exhibits good thermal stability up to approximately 200 °C in both atmospheres, an increase of about 50 °C over uncured resin. The first minor degradation event corresponds to the elimination of water through the secondary hydroxyl groups and the main degradation event corresponds to the breakage of the aliphatic chain of the polymer.

3.4.3. Coating properties

The e-CNSL/MIM5 epoxy coating was evaluated for adhesive, optical, and wettability properties. All coated panels were completely cured, with no visible defects, such as holes, bubbles, phase separation, *etc*. The dry film thickness was measured on the PosiTector® 6000 equipment and observed in the range of 193 ± 68 μm.

The gloss of coating was measured with a digital gloss meter at 60° and was observed in the range of 132–144 GU. The use of CNSL provided a higher gloss to coating when compared to commercial coating DGEBA (123–128 GU) and other bio-based blends with cardanol, reported in literature [44,45].

Regarding the hydrophobicity property, contact angle allows to evaluate the wetting behavior of surfaces. For the surface to be hydrophobic, the WCA needs to be greater than 90° [46]. The WCA measured for coating was 78.9° ± 0.8. Although a more hydrophobic character was expected for CNSL-based coating due to the aliphatic chains of cardanol and cardol, the contact angle showed a hydrophilic character. This result can be attributed to the presence of secondary hydroxyl groups formed from the opening of epoxy rings that can interact with water through hydrogen bonding. On the other hand, when compared to our previous report [27], there was an increase in hydrophobicity when using aliphatic and cycloaliphatic amine-based curing agents.

Table 3
Gel content and thermal properties of e-CNSL resin and e-CNSL/MIM5 coating.

Sample	Gel content (%)	T_g (°C)	$T_{d5\%}$ (°C)	$T_{d30\%}$ (°C)	T_{dmax} (°C)
e-CNSL	–	–	284 (N_2)	371 (N_2)	443 (N_2)
e-CNSL/MIM5	95.4 ± 0.3	30	300 (N_2)/ 295 (Air)	387 (N_2)/ 407 (Air)	433 (N_2)/ 418 (Air)

3.5. Corrosion resistance properties

3.5.1. Immersion test

Electrochemical impedance spectroscopy was used to investigate the electrochemical responses and anti-corrosion characteristics of CNSL-based epoxy coating. EIS measurements were performed periodically for 35 days after submitting the coated panels to a 3.5% NaCl solution. To achieve a stable environment, an open circuit potential (OCP) was obtained for 30 min before measurements. The results were displayed using Nyquist and Bode plots (Figs. 8 and 9).

According to literature on EIS data analysis, the impedance module at low frequency (impedance at 0.01 Hz, $|Z|_{0,01Hz}$) can be used to qualitatively evaluate the protective properties of organic coatings. Thus, as a parameter, coatings with $|Z|_{0.01Hz}$ above 10^8 Ω.cm^2 provide high protection properties, while those with $|Z|_{0.01Hz}$ below 10^6 Ω.cm^2 provide low performance protection for carbon steel substrates [47–49].

Fig. 8 shows the degradation process of e-CNSL/MIM5 coating as a function of immersion time in a 3.5% NaCl solution. In the 0.5 h curve on the Nyquist graph, the coating presents a very capacitive arc and a value of $|Z|_{0.01Hz}$ in Bode spectrum is 5.88 × 10^{10} Ω.cm^2, exhibiting a high barrier property of coating for substrate. With immersion time up to 336 h, the spectra are characterized with a single capacitive arc in which the diameter gradually decreases due to water absorption.

In the Bode graphs (Fig. 9), the $|Z|_{0.01Hz}$ value decreased from 5.88 × 10^{10} Ω.cm^2 to 3.63 × 10^8 Ω.cm^2 during 0.5–336 h, indicating that the barrier performance of coating was decreased. The phase angles also

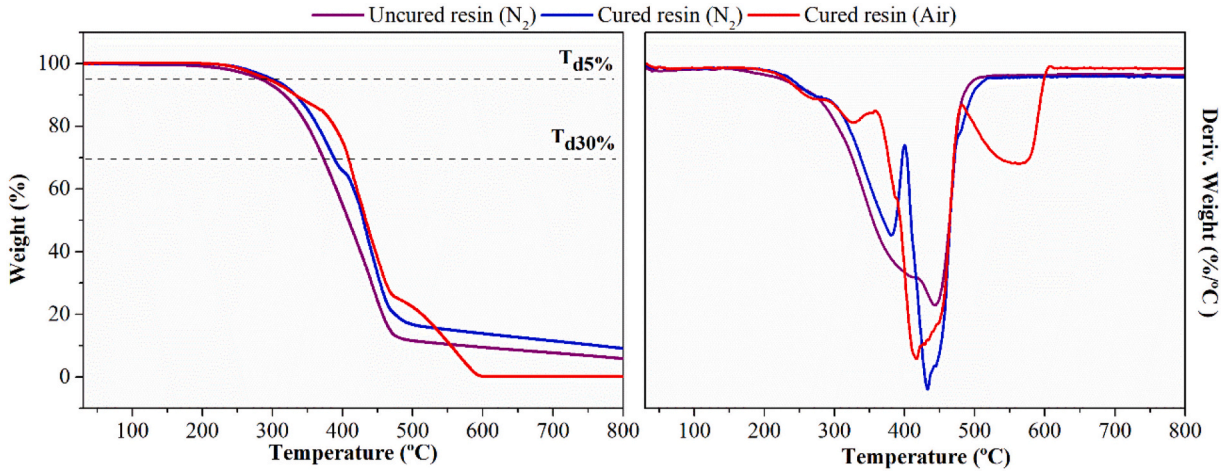

Fig. 7. TGA curves e-CNSL and e-CNSL/MIM5 under N_2 and Air.

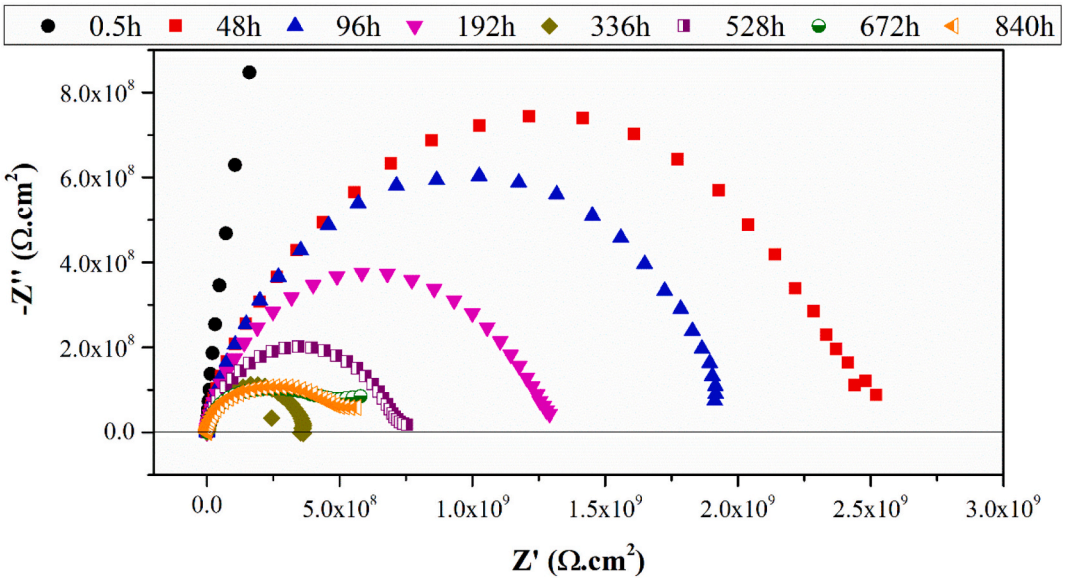

Fig. 8. Nyquist plot as a function of immersed time.

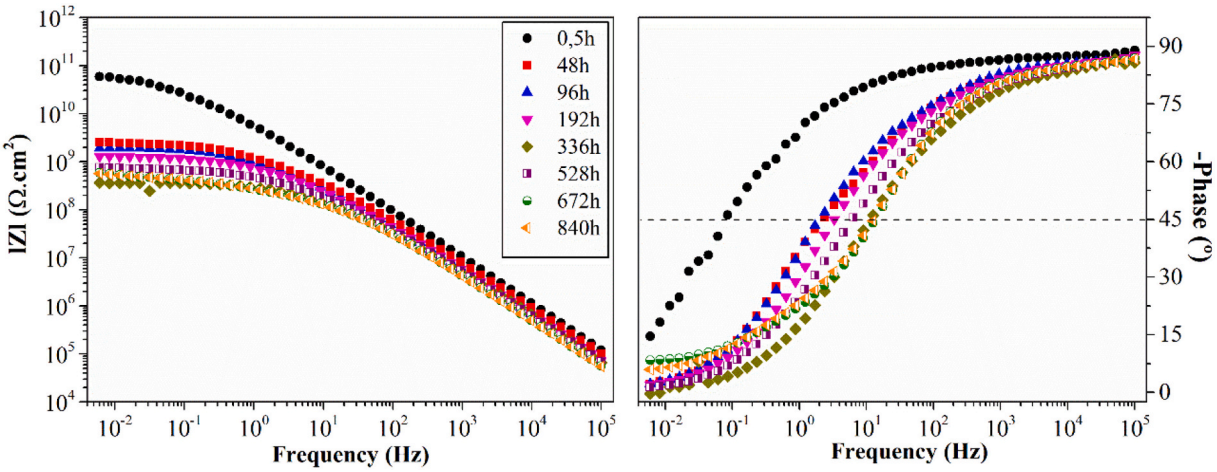

Fig. 9. Evaluation of degradation over time by Bode and Phase plot.

gradually decreased showing only a time constant, indicating that only one process occurred during the analysis, which was the diffusion of the electrolyte through the coating.

When the immersion time reaches 528 h, there is a slight increase in $|Z|_{0.01Hz}$ reaching 7.54 × 10^8 Ω.cm^2 and in subsequent immersion times. Nyquist graph (Fig. 8) shows that there is a tendency for formation of a second arc. This may have probably occurred due to the formation of corrosion products on steel surface and its blocking action on porosity of coating [47]. However, the phase angles do not show appearance of a new time constant.

Another way to better assess the changes that occurred in coating during different immersion times is to use the breakpoint frequency, where it is defined as frequency at a phase angle of −45° [9]. The increase in breakpoint frequency corresponds to increase in resistive area and, consequently, decrease in capacitive area of coating.

In this way, with respect to area under Bode graph (impedance and phase angle as a function of frequency), coating can be classified into three classes: a high-resistance coating where the whole area under the Bode plot are recognized as capacitive regions, an intermediate coating that undergoes corrosion where there is a combination of capacitive and resistive regions, and coating failure for areas where only resistive regions are observed below the Bode plot [50].

Thus, based on EIS results, the coating developed under immersion as a function of time can be classified as an intermediate coating presenting an area under Bode chart with very capacitive regions at the beginning, but over a long period of exposure capacitive/resistive regions were predominant.

3.5.2. *Salt spray and adhesion test*

Salt spray test is an accelerated test that can simulate the deposition of moisture particles (and dissolved salts) in coastal atmospheric environments. Steel panels with e-CNSL/MIM5 epoxy coating were subjected to test for 33 days. The panels were removed every 5 or 7 days for EIS measurements in a 3.5% NaCl solution (Fig. 10).

From the Bode modulus plot (Fig. 10) it is possible to observe that the $|Z|_{0.01Hz}$ value of e-CNSL/MIM5 coating decreased to 1.26 × 10^9 Ω.cm^2 after 7 days and remained degrading more slowly reaching end of the test at 5.02 × 10^8 Ω.cm^2. This occurs due to the penetration of the electrolyte in the coating and, consequently, the resistance decreases and the capacitance of coating increases. In short, the coating developed when subjected to both immersion test and salt spray test maintained its barrier properties without showing significant changes.

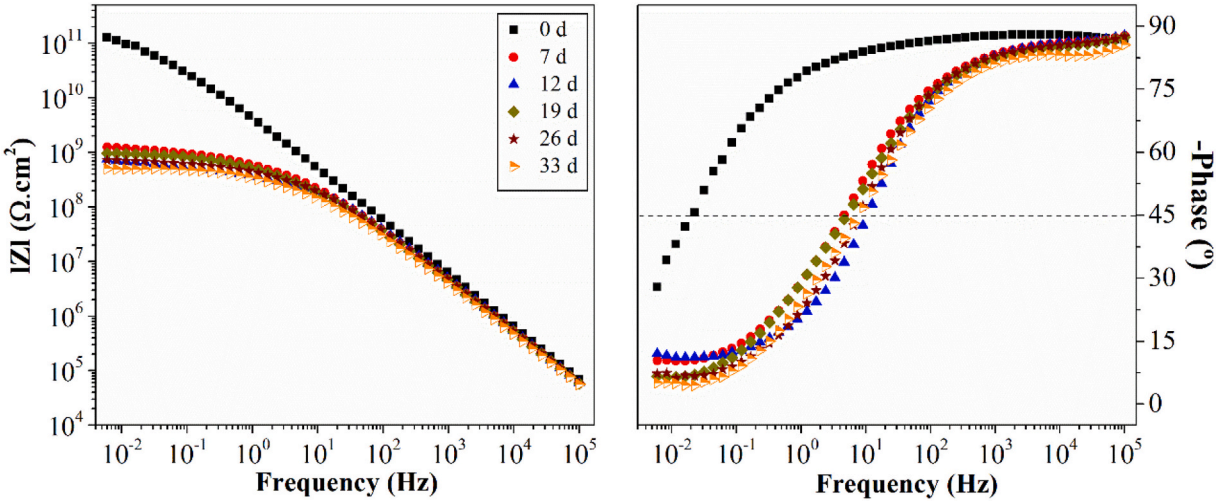

Fig. 10. Impedance of e-CNSL/MIM5 coating applied to carbon steel. Results obtained after 0, 7, 12, 19, 26 and 33 days in salt spray test.

In Fig. 10 it is clearly seen that the coating showed an abrupt increase in breakpoint frequency between 0 and 7 days, which corresponds to a microscopic delamination under coating [1,51]. After this period, it is noted that there is no worsening of delamination, the breakpoint frequency decreases slowly. Thus, the coating remained with intermediate protection behavior.

In fact, a high resistance or impedance does not always characterize the high performance of a coating. There are other properties that involve the performance of a coating against corrosion, for example, containment of corrosion in defective areas and adhesion [49].

Thus, linked to EIS monitoring, the developed coating also had its adhesive property evaluated by Pull-Off adhesion test during salt spray test and visual assessment of progress of corrosion in the risk. Fig. 11 shows the adhesion test performed before, after 14 and 33 days of exposure.

The test result is given by the applied force and nature of the failure that can be observed in ASTM 4541-17, being of two types: cohesive and adhesive. The substrate is coded as A, coating as B, adhesive glue as Y, and dolly as Z. Adhesive failure occurs when there is separation between two layers (A/B - metallic substrate/coating, B/Y - adhesive coating/glue, Y/Z - adhesive glue/dolly). Failure of the A/B adhesive is undesirable as it indicates that there was not good adhesion between the coating and the metallic substrate. However, cohesive failure occurs when adhesion at the interface exceeds the cohesion of the coating layer. This type of failure indicates the existence of an optimal adhesion force [27,52].

Initially, coating presented a rupture stress value of 16 ± 0.7 MPa, presenting mostly cohesive failure. Epoxy coatings have a high rupture stress due to the presence of hydrogen bonding at metal/epoxy interface [53]. In epoxy resins, hydroxyl groups are responsible for this type of interaction [54]. The coating used has a high degree of curing which gives it a greater amount of hydroxyl groups formed and, consequently, greater adhesion strength.

After 336 h, the adhesion value was 9 ± 0.8 MPa with predominantly cohesive or glue failure. With end of salt spray test, the last adhesion test was carried out with a result of 6 ± 1.2 MPa. The degradation of coating by exposure to salt spray significantly reduces the adhesion strength of coating to metallic substrate. This confirms the occurrence of delamination observed by increase in breakpoint frequency, although it still works perfectly as a barrier preventing corrosion from occurring under film, as can be seen in Fig. 11c, because it always presents failure of a cohesive nature.

Fig. 12 shows the results of visual assessment in the risk region during the salt spraying of e-CNSL/MIM5 coating. The results showed that the coating had a high protection performance against the progress of corrosion with a behavior capable of withstanding the delamination

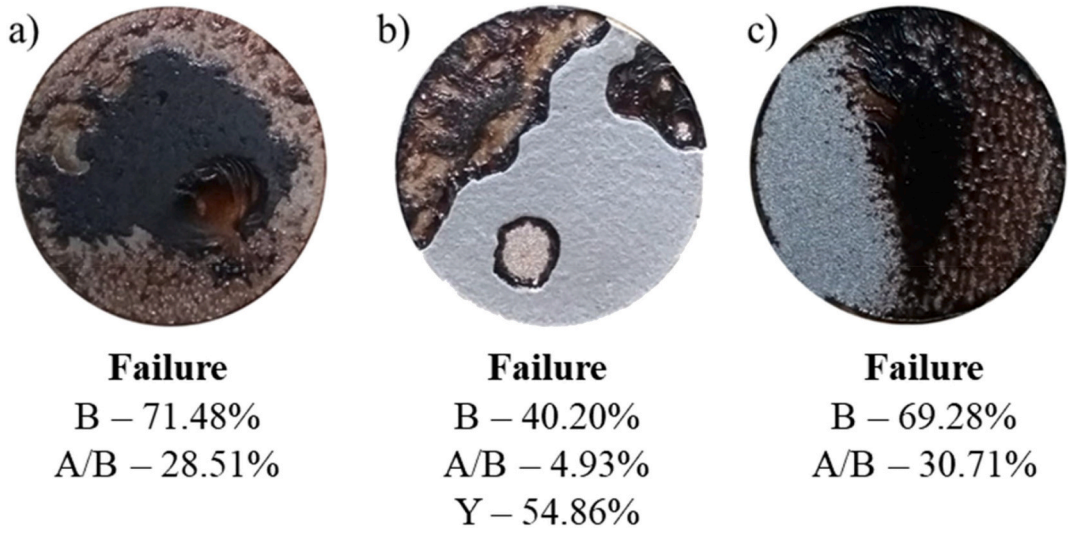

Fig. 11. Results of the pull-off adherence test during 0, 14 and 33 days salt spray test exposure.

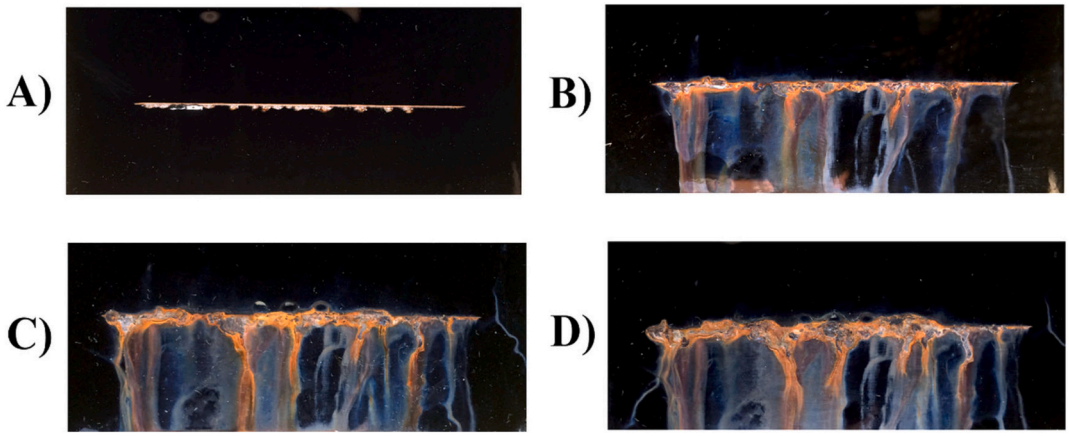

Fig. 12. Salt spray images of e-CNSL/MIM5 coating (a) on day 0 (b) in 19 days (c) in 26 days (d) in 33 days.

and the formation of rust in the areas close to risks. Its indicates that adhesive forces between coating and metallic substrate were very strong preventing the entry of electrolyte through coating/metal interface, thus preventing the spread of corrosion. In addition, this observation is in agreement with the results of the EIS, which confirms the stability of e-CNSL/MIM5 coating system throughout test period.

3.5.3. Humidity exposure

The samples exposed to the humidity chamber are shown in Fig. 13. Coatings were evaluated according to ASTM D714 - 02. After 19 days the e-CNSL/MIM5 coating begins to show a rough appearance. This roughness increases with long exposure period (37–44 days) and distorts the reflected image. The appearance of bubbles occurs at 27 days, and at 44 days. The density of bubbles reaches half surface of coating and this profile is coded as M-8 according to ASTM D714 - 02, where the frequency of bubbles is average and size of the bubbles represents the smallest size easily seen with naked eye. For this coating, it was not possible to observe values of degree of rust due to your dark color.

Organic coatings are permeable to oxygen and water due to the action of osmotic pressure which makes saturated humidity test more critical for bubble formation than the salt spray test [55]. The coating acquires the properties of a semipermeable membrane, leading to the destruction of its passive property.

Another important point is to evaluate the effect of temperature on the properties of organic coating. When glass transition temperatures are exceeded, their properties are changed [49]. The *Tg* obtained by DSC for e-CNSL/MIM5 coating was 30 °C in dry conditions. As the test was carried out at 40 °C, that is, above the *Tg* of the coating, this may have increased water absorption and, as a consequence, the formation of bubbles. The literature reports that epoxy coatings when saturated with water can suffer a decrease of up to 20 °C in *Tg*, with that, coating suffers a plasticizing effect due to the absorption of water, decreasing its barrier property [56].

4. Conclusions

This work is a direct contribution to the study and development of new sustainable materials, using cashew nutshell liquid, as a bio-based and eco-friendly raw material. CNSL had its efficiency proven as an alternative to petrochemical sources in the field of organic coatings produced from epoxy resins, showing good performance in controlling or mitigating the degradation of metallic substrates.

The use of 1-methylimidazole, in catalytic amounts, was sufficient to promote the cure of the one-component epoxy-phenol system, as well to

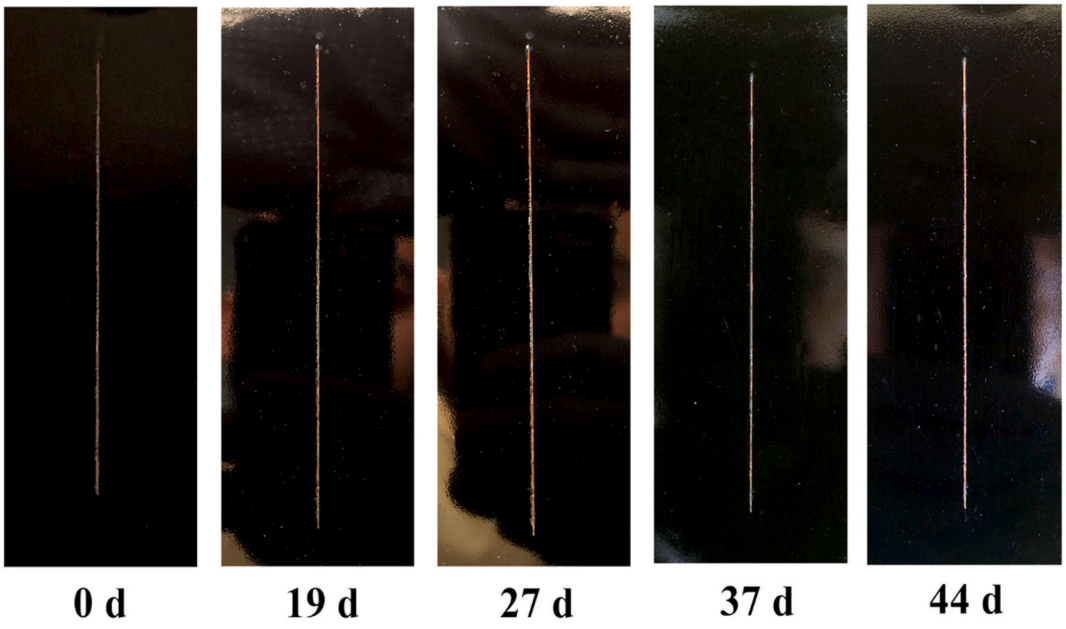

Fig. 13. Humidity resistance of e-CNSL/MIM5 coating during 0, 19, 27, 37 and 44 days of exposure.

providing a low cure temperature. In this way, a CNSL-based material was obtained with good thermal stability, high crosslink density, and high glass transition temperature compared to the same epoxy resin cured with conventional amines in two-component systems produced in our previous work. The organic coating showed strong pull-off adhesion and a notable ability to protect against corrosion in highly aggressive environments, such as salt spray and saturated moisture.

CRediT authorship contribution statement

We describe contributions to this paper using CRediT:

- **Lucas R. R. da Silva**: Writing – Original Draft/Investigation
- **Bruna A. Carvalho**: Investigation
- **Rita C. S. Pereira**: Investigation
- **Otilio B. F. Diógenes**: Investigation
- **Ursula C. Pereira**: Investigation
- **Kássia T. da Silva**: Writing – Original Draft/Investigation
- **Selma Elaine Mazzetto**: Funding Acquisition/Project Administration
- **Walney S. Araujo**: Funding Acquisition/Writing – Review & Editing/Supervision/Conceptualization
- **Diego Lomonaco**: Funding Acquisition/Writing – Review & Editing/Supervision/Conceptualization

Declaration of competing interest

The authors declare that they have no known competing financial interests or personal relationships that could have appeared to influence the work reported in this paper.

Acknowledgments

The authors acknowledge Brazilian agencies Conselho Nacional de Desenvolvimento Científico e Tecnológico - CNPq (407291/2018-0), Coordenação de Aperfeiçoamento de Pessoal de Nível Superior - CAPES (Finance Code 001/PROEX 23038.000509/2020-82) and Fundação Cearense de Apoio ao Desenvolvimento Científico e Tecnológico - FUNCAP for the financial support; CENAUREMN (Centro Nordestino de Aplicação da Ressonância Magnética Nuclear at Fortaleza, Brazil) for the NMR analyses; and Embrapa (Empresa Brasileira de Pesquisa Agropecuária) for the WCA analyses.

References

[1] L. Cheng, C. Liu, H. Wu, H. Zhao, F. Mao, L. Wang, A mussel-inspired delivery system for enhancing self-healing property of epoxy coatings, J. Mater. Sci. Technol. 80 (2021) 36–49, https://doi.org/10.1016/j.jmst.2020.10.075.
[2] S.B. Lyon, R. Bingham, D.J. Mills, Advances in corrosion protection by organic coatings: what we know and what we would like to know, Prog. Org. Coat. 102 (2017) 2–7, https://doi.org/10.1016/j.porgcoat.2016.04.030.
[3] F. Zhang, L. Zhang, M. Yaseen, K. Huang, A review on the self-healing ability of epoxy polymers, J. Appl. Polym. Sci. 138 (2021) 1–14, https://doi.org/10.1002/app.50260.
[4] B. Yang, Y. Mao, Y. Zhang, G. Bian, L. Zhang, Y. Wei, Q. Jiang, Y. Qiu, W. Liu, A novel liquid imidazole-copper (II) complex as a thermal latent curing agent for epoxy resins, Polymer (Guildf) 178 (2019), 121586, https://doi.org/10.1016/j.polymer.2019.121586.
[5] E. Feghali, D.J. Van De Pas, A.J. Parrott, K.M. Torr, Biobased epoxy thermoset polymers from depolymerized native hardwood lignin, ACS Macro Lett. 9 (2020) 1155–1160, https://doi.org/10.1021/acsmacrolett.0c00424.
[6] Y. Qi, Z. Weng, K. Zhang, J. Wang, S. Zhang, C. Liu, X. Jian, Magnolol-based bio-epoxy resin with acceptable glass transition temperature, processability and flame retardancy, Chem. Eng. J. 387 (2020), 124115, https://doi.org/10.1016/j.cej.2020.124115.
[7] H. Nabipour, X. Wang, L. Song, Y. Hu, A high performance fully bio-based epoxy thermoset from a syringaldehyde-derived epoxy monomer cured by furan-derived amine, Green Chem. 23 (2021) 501–510, https://doi.org/10.1039/d0gc03451g.
[8] Y. Zhang, Y. Lei, H. Lu, L. Shi, P. Wang, Z. Ali, J. Li, Electrochemical detection of bisphenols in food: a review, Food Chem. 346 (2021), 128895, https://doi.org/10.1016/j.foodchem.2020.128895.
[9] S. Ammar, A.W.M. Iling, K. Ramesh, S. Ramesh, Development of fully organic coating system modified with epoxidized soybean oil with superior corrosion protection performance, Prog. Org. Coat. 140 (2020), 105523, https://doi.org/10.1016/j.porgcoat.2019.105523.
[10] P.A. Parvathy, S.K. Sahoo, Hydrophobic, moisture resistant and biorenewable paper coating derived from castor oil based epoxy methyl ricinoleate with repulpable potential, Prog. Org. Coat. 158 (2021), 106347, https://doi.org/10.1016/j.porgcoat.2021.106347.
[11] S. Nikafshar, J. Wang, K. Dunne, P. Sangthonganotai, M. Nejad, Choosing the right lignin to fully replace bisphenol A in epoxy resin formulation, ChemSusChem 14 (2021) 1184–1195, https://doi.org/10.1002/cssc.202002729.
[12] E. Kinaci, E. Can, J.J. La Scala, G.R. Palmese, Epoxidation of cardanol's terminal double bond, Polymers (Basel) 12 (2020) 1–12, https://doi.org/10.3390/POLYM12092104.
[13] A.F.J. Uchoa, W.S. Rocha, J.P.M. Feitosa, D.H.A. Brito, L.M. Gondim, N.M.P. S. Ricardo, J.B. Soares, S.A. Soares, Exploiting epoxidized cashew nut shell liquid as a potential bio-additive to improve asphalt binder performance, J. Clean. Prod. 314 (2021), https://doi.org/10.1016/j.jclepro.2021.128061.
[14] K.de P. Costa, B.M. de Viveiros, M.A.S.Schmidt Junior, P.A.Z. Suarez, M.J. C. Rezende, Chemical transformations in technical cashew nut shell liquid and isolated mixture of cardanols, evaluation of the antioxidant activity and thermal stability of the products for use in pure biodiesel, Fuel 235 (2019) 1010–1018, https://doi.org/10.1016/j.fuel.2018.08.111.
[15] S. Caillol, Cardanol: a promising building block for biobased polymers and additives, Curr. Opin. Green Sustain. Chem. 14 (2018) 26–32, https://doi.org/10.1016/j.cogsc.2018.05.002.
[16] J. Mgaya, G.B. Shombe, S.C. Masikane, S. Mlowe, E.B. Mubofu, N. Revaprasadu, Cashew nut shell: a potential bio-resource for the production of bio-sourced chemicals, materials and fuels, Green Chem. 21 (2019) 1186–1201, https://doi.org/10.1039/c8gc02972e.
[17] P. Sharma, V.K. Gaur, R. Sirohi, C. Larroche, S.H. Kim, A. Pandey, Valorization of cashew nut processing residues for industrial applications, Ind. Crop. Prod. 152 (2020), 112550, https://doi.org/10.1016/j.indcrop.2020.112550.
[18] A. Greco, F. Ferrari, A. Maffezzoli, Mechanical properties of poly(lactid acid) plasticized by cardanol derivatives, Polym. Degrad. Stab. 159 (2019) 199–204, https://doi.org/10.1016/j.polymdegradstab. 2018.11.028.
[19] D. Hou, S. Wang, J. Chang, Z. Xu, Q. Zeng, Z. Wang, Y. Yang, J. Yan, Y. Chen, Cardanol with a covalently attached organophosphate moiety as a halogen-free, intrinsically flame-retardant PVC bio-plasticizer, Fibers Polym. 21 (2020) 1649–1656, https://doi.org/10.1007/s12221-020-9918-4.
[20] M.O. de Almeida, L.R.R. Silva, L.R.V. Kotzebue, F.J.N. Maia, J.S.R. Acero, G. Mele, S.E. Mazzetto, A. Sinatora, D. Lomonaco, Development of fully bio-based lubricants from agro-industrial residues under environmentally friendly processes, Eur. J. Lipid Sci. Technol. 122 (2020) 1–11, https://doi.org/10.1002/ejlt.201900424.
[21] K. Wazarkar, A.S. Sabnis, Phenalkamine curing agents for epoxy resin: characterization and structure property relationship, Pigment Resin Technol. 47 (2018) 281–289, https://doi.org/10.1108/PRT-08-2017-0071.
[22] N.L. Jadhav, S.K.C. Sastry, D.V. Pinjari, Energy efficient room temperature synthesis of cardanol-based novolac resin using acoustic cavitation, Ultrason. Sonochem. 42 (2018) 532–540, https://doi.org/10.1016/j.ultsonch.2017.12.001.
[23] E. Kinaci, E. Can, J.J. La Scala, G.R. Palmese, Influence of epoxidized cardanol functionality and reactivity on network formation and properties, Polymers (Basel) 12 (2020) 1–14, https://doi.org/10.3390/polym12091956.
[24] Y. Ecochard, M. Decostanzi, C. Negrell, R. Sonnier, S. Caillol, Cardanol and eugenol based flame retardant epoxy monomers for thermostable networks, Molecules 24 (2019) 1–21, https://doi.org/10.3390/molecules24091818.
[25] V. Somisetti, R. Narayan, R.V.S.N. Kothapalli, Multifunctional polyurethane coatings derived from phosphated cardanol and undecylenic acid based polyols, Prog. Org. Coat. 134 (2019) 91–102, https://doi.org/10.1016/j.porgcoat.2019.04.077.
[26] P.P. Kumar, R. Paramashivappa, P.J. Vithayathil, P.V.S. Rao, A.S. Rao, Process for isolation of cardanol from technical cashew (Anacardium occidentale l.) nut shell liquid, J. Agric. Food Chem. 50 (2002) 4705–4708, https://doi.org/10.1021/jf020224w.
[27] L.R.R. da Silva, F. Avelino, O.B.F. Diogenes, V.de O.F. Sales, K.T. da Silva, W. S. Araujo, S.E. Mazzetto, D. Lomonaco, Development of BPA-free anticorrosive epoxy coatings from agroindustrial waste, Prog. Org. Coat. 139 (2020) 105449, https://doi.org/10.1016/j.porgcoat.2019.105449.
[28] M. Tubino, J.A. Aricetti, A green potentiometric method for the determination of the iodine number of biodiesel, Fuel 103 (2013) 1158–1163, https://doi.org/10.1016/j.fuel.2012.10.011.
[29] Y. Tian, M. Ke, X. Wang, G. Wu, J. Zhang, J. Cheng, A resveratrol-based epoxy resin with ultrahigh Tg and good processability, Eur. Polym. J. 147 (2021), 110282, https://doi.org/10.1016/j.eurpolymj.2021.110282.
[30] A.S. Mora, M. Decostanzi, G. David, S. Caillol, Cardanol-based epoxy monomers for high thermal properties thermosets, Eur. J. Lipid Sci. Technol. 121 (2019) 1–8, https://doi.org/10.1002/ejlt.201800421.
[31] Z. Liu, J. Chen, G. Knothe, X. Nie, J. Jiang, Synthesis of epoxidized cardanol and its antioxidative properties for vegetable oils and biodiesel, ACS Sustain. Chem. Eng. 4 (2016) 901–906, https://doi.org/10.1021/acssuschemeng.5b00991.
[32] L.L. Monteavaro, E.O. Da Silva, A.P.O. Costa, D. Samios, A.E. Gerbase, C. L. Petzhold, Polyurethane networks from formiated soy polyols: synthesis and mechanical characterization, J. Am. Oil Chem. Soc. 82 (2005) 365–371, https://doi.org/10.1007/s11746-005-1079-0.

[33] V. Ladmiral, R. Jeannin, K. Fernandes Lizarazu, J. Lai-Kee-Him, P. Bron, P. Lacroix-Desmazes, S. Caillol, Aromatic biobased polymer latex from cardanol, Eur. Polym. J. 93 (2017) 785–794, https://doi.org/10.1016/j.eurpolymj.2017.04.003.
[34] B. Briou, S. Caillol, J.J. Robin, V. Lapinte, Non-endocrine disruptor effect for cardanol based plasticizer, Ind. Crop. Prod. 130 (2019) 1–8, https://doi.org/10.1016/j.indcrop.2018.12.060.
[35] R. Turco, R. Tesser, V. Russo, T. Cogliano, M. Di Serio, E. Santacesaria, Epoxidation of linseed oil by performic acid produced in situ, Ind. Eng. Chem. Res. 60 (2021) 16607–16618, https://doi.org/10.1021/acs.iecr.1c02212.
[36] S.M. Danov, O.A. Kazantsev, A.L. Esipovich, A.S. Belousov, A.E. Rogozhin, E. A. Kanakov, Recent advances in the field of selective epoxidation of vegetable oils and their derivatives: a review and perspective, Catal. Sci. Technol. 7 (2017) 3659–3675, https://doi.org/10.1039/c7cy00988g.
[37] A. Freites Aguilera, J. Rahkila, J. Hemming, M. Nurmi, G. Torres, T. Razat, P. Tolvanen, K. Eränen, S. Leveneur, T. Salmi, Epoxidation of tall oil catalyzed by an ion exchange resin under conventional heating and microwave irradiation, Ind. Eng. Chem. Res. 59 (2020) 10397–10406, https://doi.org/10.1021/acs.iecr.0c01288.
[38] L. Shechter, J. Wynstra, Glycidyl ether reactions with alcohols, phenols, carboxylic acids, and acid anhydrides, Ind. Eng. Chem. 48 (1956) 86–93, https://doi.org/10.1021/ie50553a028.
[39] C.P.R. Nair, Advances in addition-cure phenolic resins, Prog. Polym. Sci. 29 (2004) 401–498, https://doi.org/10.1016/j.progpolymsci.2004.01.004.
[40] M. Qi, Y.J. Xu, W.H. Rao, X. Luo, L. Chen, Y.Z. Wang, Epoxidized soybean oil cured with tannic acid for fully bio-based epoxy resin, RSC Adv. 8 (2018) 26948–26958, https://doi.org/10.1039/c8ra03874k.
[41] X.M. Ding, L. Chen, D.M. Guo, B.W. Liu, X. Luo, Y.F. Lei, H.Y. Zhong, Y.Z. Wang, Controlling cross-linking networks with different imidazole accelerators toward high-performance epoxidized soybean oil-based thermosets, ACS Sustain. Chem. Eng. 9 (2021) 3267–3277, https://doi.org/10.1021/acssuschemeng.0c08852.
[42] Y. Zhang, F. Ferdosian, Z. Yuan, C.C. Xu, Sustainable glucose-based phenolic resin and its curing with a DGEBA epoxy resin, J. Taiwan Inst. Chem. Eng. 71 (2017) 381–387, https://doi.org/10.1016/j.jtice.2016.11.025.
[43] R. Liu, X. Zhang, J. Zhu, X. Liu, Z. Wang, J. Yan, UV-curable coatings from multiarmed cardanol-based acrylate oligomers, ACS Sustain. Chem. Eng. 3 (2015) 1313–1320, https://doi.org/10.1021/acssuschemeng.5b00029.
[44] E. Darroman, N. Durand, B. Boutevin, S. Caillol, Improved cardanol derived epoxy coatings, Prog. Org. Coat. 91 (2016) 9–16, https://doi.org/10.1016/j.porgcoat.2015.11.012.
[45] E. Darroman, N. Durand, B. Boutevin, S. Caillol, New cardanol/sucrose epoxy blends for biobased coatings, Prog. Org. Coat. 83 (2015) 47–54, https://doi.org/10.1016/j.porgcoat.2015.02.002.
[46] P. Nguyen-Tri, H.N. Tran, C.O. Plamondon, L. Tuduri, D.V.N. Vo, S. Nanda, A. Mishra, H.P. Chao, A.K. Bajpai, Recent progress in the preparation, properties and applications of superhydrophobic nano-based coatings and surfaces: a review, Prog. Org. Coat. 132 (2019) 235–256, https://doi.org/10.1016/j.porgcoat.2019.03.042.
[47] C. Xing, W. Wang, S. Qu, Y. Tang, X. Zhao, Y. Zuo, Degradation of zinc-rich epoxy coating in 3.5% NaCl solution and evolution of its EIS parameters, J. Coat. Technol. Res. 18 (2021) 843–860, https://doi.org/10.1007/s11998-020-00448-8.
[48] A. Amirudin, D. Thieny, Application of electrochemical impedance spectroscopy to study the degradation of polymer-coated metals, Prog. Org. Coat. 26 (1995) 1–28, https://doi.org/10.1016/0300-9440(95)00581-1.
[49] I.C.P. Margarit-Mattos, EIS and organic coatings performance: revisiting some key points, Electrochim. Acta 354 (2020), 136725, https://doi.org/10.1016/j.electacta.2020.136725.
[50] E. Akbarinezhad, M. Bahremandi, H.R. Faridi, F. Rezaei, Another approach for ranking and evaluating organic paint coatings via electrochemical impedance spectroscopy, Corros. Sci. 51 (2009) 356–363, https://doi.org/10.1016/j.corsci.2008.10.029.
[51] J.G. Wen, W. Geng, H.Z. Geng, H. Zhao, L.C. Jing, X.T. Yuan, Y. Tian, T. Wang, Y. J. Ning, L. Wu, Improvement of corrosion resistance of waterborne polyurethane coatings by covalent and noncovalent grafted graphene oxide nanosheets, ACS Omega 4 (2019) 20265–20274, https://doi.org/10.1021/acsomega.9b02687.
[52] O.B.F. Diógenes, D.R. de Oliveira, L.R.R. da Silva, Í.G. Pereira, S.E. Mazzetto, W. S. Araujo, D. Lomonaco, Development of coal tar-free coatings: acetylated lignin as a bio-additive for anticorrosive and UV-blocking epoxy resins, Prog. Org. Coat. 161 (2021) 1–9, https://doi.org/10.1016/j.porgcoat.2021.106533.
[53] C. Yi, P. Rostron, N. Vahdati, E. Gunister, A. Alfantazi, Curing kinetics and mechanical properties of epoxy based coatings: the influence of added solvent, Prog. Org. Coat. 124 (2018) 165–174, https://doi.org/10.1016/j.porgcoat.2018.08.009.
[54] A.M. Atta, H.A. Al-Hodan, R.S.A. Hameed, A.O. Ezzat, Preparation of green cardanol-based epoxy and hardener as primer coatings for petroleum and gas steel in marine environment, Prog. Org. Coat. 111 (2017) 283–293, https://doi.org/10.1016/j.porgcoat.2017.06.002.
[55] I. Stojanović, B. Židov, O. Travkova, D. Grigoriev, Enhanced protective performance of waterborne, microcontainers-doped coatings in harsh environments, Prog. Org. Coat. 157 (2021), 106273, https://doi.org/10.1016/j.porgcoat.2021.106273.
[56] I.C.P. Margarit-Mattos, F.A.R. Agura, C.G. Silva, W.A. Souza, J.P. Quintela, V. Solymossy, Electrochemical impedance aiding the selection of organic coatings for very aggressive conditions, Prog. Org. Coat. 77 (2014) 2012–2023, https://doi.org/10.1016/j.porgcoat.2014.04.006.